doi:10.1006/jmbi.2000.3806 available online at http://www.idealibrary.com on IDEAL® *J. Mol. Biol.* (2000) **299**, 1035–1049

JMB

Crystal Structure of Dodecameric Vanadium-dependent Bromoperoxidase from the Red Algae *Corallina officinalis*

Michail N. Isupov[1], Andrew R. Dalby[1], Amanda A. Brindley[1] Yoshikazu Izumi[2], Tadashi Tanabe[3], Garib N. Murshudov[4,5] and Jennifer A. Littlechild[1]*

[1]*Schools of Chemistry and Biological Sciences, University of Exeter, Stocker Road, Exeter EX4 4QD, UK*

[2]*Department of Biotechnology Faculty of Engineering, Tottori University, Tottori, Koyama-cho 980, Japan*

[3]*Department of Pharmacology National Cardiovascular Centre Research Institute, Fujishiro-day, Suita, 565-8565, Japan*

[4]*Department of Chemistry University of York, Heslington York, Y01 5DD, UK*

[5]*CLRC, Daresbury Laboratory Daresbury, Warrington WA4 4AD, UK*

**Corresponding author*

The three-dimensional structure of the vanadium bromoperoxidase protein from the marine red macroalgae *Corallina officinalis* has been determined by single isomorphous replacement at 2.3 Å resolution. The enzyme subunit is made up of 595 amino acid residues folded into a single $\alpha + \beta$ domain. There are 12 bromoperoxidase subunits, arranged with 23-point group symmetry. A cavity is formed by the N terminus of each subunit in the centre of the dodecamer. The subunit fold and dimer organisation of the *Cor. officinalis* vanadium bromoperoxidase are similar to those of the dimeric enzyme from the brown algae *Ascophyllum nodosum*, with which it shares 33 % sequence identity. The different oligomeric state of the two algal enzymes seems to reflect separate mechanisms of adaptation to harsh environmental conditions and/or to chemically active substrates and products. The residues involved in the vanadate binding are conserved between the two algal bromoperoxidases and the vanadium chloroperoxidase from the fungus *Curvularia inaequalis*. However, most of the other residues forming the active-site cavity are different in the three enzymes, which reflects differences in the substrate specificity and stereoselectivity of the reaction. A dimer of the *Cor. officinalis* enzyme partially superimposes with the two-domain monomer of the fungal enzyme.

© 2000 Academic Press

Keywords: vanadium; haloperoxidase; dodecamer; enzyme structure; vanadium binding site

Introduction

Many naturally occurring halogenated organic compounds have been isolated; this list is constantly increasing (Gribble, 1992). They are produced by seaweeds, sponges, lichens and fungi and are thought to be associated with defence mechanisms preventing the organism from being eaten by predators and to aid colonisation in natural habitats (Simons *et al.*, 1995). The addition of halide to nucleophilic organic substrates in the presence of hydrogen peroxide is catalysed by haloperoxidases. These enzymes have been isolated from a diverse range of organisms (Ahern *et al.*, 1980; Manthey & Hager, 1981; Van Peé & Lingens, 1985; Zeng & Fenna, 1992; Itoh *et al.*, 1994). Haloperoxidases are named according to the most electronegative halogen they oxidise (Hemrika *et al.*, 1997). On the basis of their cofactor requirement they are classified into the three groups: heme-containing, vanadium-containing and metal-free haloperoxidases (Hemrika *et al.*, 1997).

A bromoperoxidase enzyme with an absolute requirement for vanadium (VBPO) was first isolated from the brown macro-algae *Ascophyllum nodosum* (Wever *et al.*, 1985). One molecule of vanadate per subunit was shown to be required for the enzyme activity (Wever *et al.*, 1988). EPR studies (Wever *et al.*, 1988) and K-edge X-ray absorption

Abbreviations used: VBPO, vanadium bromoperoxidase; AVBPO, *Ascophyllum nodosum* VBPO; CVBPO, *Corallina officinalis* VBPO; H-bond, hydrogen bond; NCS, non-crystallographic symmetry; F_o, observed structure factors; F_c, calculated structure factors.

E-mail address of the corresponding author: J.A.Littlechild@exeter.ac.uk

0022-2836/00/041035–15 $35.00/0

© 2000 Academic Press

studies (Kusthardt *et al*., 1993) on the bromoperoxidase from *A. nodosum* (AVBPO) showed that the oxidation state of the metal was vanadium V. The redox state of the metal is not thought to change during turnover of the enzyme. It has been proposed that the function of the vanadium is to bind hydrogen peroxide to yield an activated peroxo intermediate, which is able to react with bromide to produce HOBr (Wever *et al*., 1988). Vanadium-dependent haloperoxidase enzymes have now been isolated from a number of marine algae (Wever *et al*., 1985; Itoh *et al*., 1986; Sheffield *et al*., 1993) and also from some lichens and fungi (Van Schijndel *et al*., 1993; Plat *et al*., 1987).

The primary amino acid sequence of the vanadium chloroperoxidases from the fungal species *Curvularia inaequalis* (Simons *et al*., 1995), *Embellisia didymospora* (Barnett *et al*., 1998) and *Drechslera biseptata* (partial sequence; Hemrika *et al*., 1997) show sequence identity in the range of 65-95 %. The two vanadium bromoperoxidases from the red macroalgae *Corallina pilulifera* (Shimonishi *et al*., 1998) show sequence identity of 91 % and the VBPOs from the brown macroalgae *Fucus distichus* (Vreeland *et al*., 1998) and *A. nodosum* (Vilter, 1995; Weyand *et al*., 1999) have a sequence identity of 86 %. The VBPO enzymes from the red algae show 32-34 % identity to those from the brown algae. There is, however, less sequence identity between the algal VBPO and the fungal vanadium chloroperoxidase enzymes. Only the catalytic C-terminal regions can be aligned with no more than 26 % identity within a 103 amino acid residue overlap. The acid phosphatases show sequence identity to the vanadium-binding site motifs in haloperoxidase enzymes (Hemrika *et al*., 1997).

The X-ray crystallographic structures of the chloroperoxidase from the fungus *Cur. inaequalis* in both the native and peroxide-bound forms have been determined (Messerschmidt & Wever, 1996; Messerschmidt *et al*., 1997). The monomer of the enzyme has two α-helical domains with a similar fold, the four α-helix bundles of each domain are related by approximately 180° rotation (Messerschmidt & Wever, 1996). The active site is located at the end of a four-α-helix cluster in the C-terminal domain, the residues of the N-terminal domain contribute to the active site. Kinetic (Hemrika *et al*., 1999) and structural (Macedo-Ribeiro *et al*., 1999) studies of mutant chloroperoxidase proteins have recently shown the importance of histidine, which forms a chemical bond to vanadate and three basic residues involved in the vanadate-binding site for this chloroperoxidase reaction. A mechanism for the halogenation reaction was proposed by Messerschmidt & Wever (1996) and this has been developed by Hemrika *et al*. (1999). The crystal structure of the dimeric VBPO from the marine brown algae *A. nodosum* (Weyand *et al*., 1999) was recently reported which reinforced the proposed mechanism for chloroperoxidase. Bromine K-edge EXAFS studies used to investigate the binding of bromide to AVBPO have suggested that the bromide ion does not coordinate to the vanadium centre, but is bound covalently to a carbon atom (Dau *et al*., 1999).

The VBPO from the red macroalgae *Cor. officinalis* (CVBPO), a seaweed found on the south Devon coast, has been isolated and characterised (Sheffield *et al*., 1993). It was suggested to be a homododecamer based on its subunit molecular mass of 64 kDa from SDS-gel electrophoresis, and a total molecular mass from equilibrium centrifugation studies of 740 kDa (Sheffield *et al*., 1993). Itoh *et al*. (1986) reported the same subunit molecular mass and the oligomer molecular mass of 790(±20) kDa for the related enzyme from *Cor. pilulifera*.

The VBPO enzymes from *Corallina* species have been shown to be thermostable, stable to organic solvents and also resistant to high concentrations of hydrogen peroxide (Sheffield *et al*., 1993; Itoh *et al*., 1986). These features make VBPO a candidate for use as an industrial catalyst in biotransformation reactions (Soedjak & Butler, 1990; Neidleman & Geigert, 1987; Sheffield *et al*., 1995). CVBPO has been shown to perform regio-specific bromination of cinnamyl substrates and aromatic heterocycles as well as the stereo-specific oxidation of pro-chiral sulphide ions (Itoh *et al*., 1987, 1988; Coughlin *et al*., 1993; Anderson *et al*., 1997).

The enzyme from *Cor. officinalis* has been crystallised in two different forms (Rush *et al*., 1995; Brindley *et al*., 1998). A cubic crystal form was grown in the presence of vanadium, and a tetragonal form was grown from ammonium phosphate. The phosphate group has been shown to compete with vanadate for binding in the enzyme active site (Hemrika *et al*., 1997). Preliminary crystallographic analysis has shown that the CVBPO dodecamer has its subunits arranged with a cubic 23-point group symmetry (Brindley *et al*., 1998). We report here the CVBPO crystal structure determined to 2.3 Å resolution in its complex with inorganic phosphate and its comparison with the AVBPO and the *Cur. inaequalis* chloroperoxidase structures.

Results and Discussion

Quality of the model

The CVBPO structure has been refined to an *R*-factor of 0.172 for all data in the resolution range 22-2.3 Å without a σ cut-off. This excluded 2.0 % of the randomly distributed reflections assigned to calculate the R_{free} of 0.227. The asymmetric unit contains six subunits. One of the molecular dyads of the CVBPO dodecamer coincides with a diagonal crystallographic 2-fold axis. The electron density allowed the positioning of all 595 amino acid residues within each subunit. The model also contains 2186 water molecules, six phosphate ions and six magnesium ions.

The dispersion-precision indicator (Murshudov & Dodson, 1997) gives an overall estimate of root

mean square error in the co-ordinates of 0.18 Å for the well-defined part of the structure. The overall *G*-factor is 0.0 as calculated by the program PROCHECK (Laskowski *et al.*, 1993) used as a measure of the stereochemical quality of the model, which is better than expected for 2.3 Å resolution. Gly482 and Pro527 are in the *cis* conformation. 93% of the non-glycine residues fall in the most favourable regions of the Ramachandran plot (Ramakrishan & Ramachandran, 1965) as defined by PROCHECK. Ala304 ($\phi = 83°$; $\psi = 11°$) and Phe371 ($\phi = -158°$; $\psi = -77°$) have unfavourable main-chain torsion angles in all six subunits. However, the electron density for these residues is unambiguous and their *B*-factors are low. Approximately 39% of the amino acid residues are in α-helices, 7% in β-sheets and 3% in 3_{10} helices.

The six subunits were rebuilt independently and were refined with strict non-crystallographic symmetry (NCS) constraints, however, these were loosened for some loops involved in crystallographic contacts. The root mean square deviation (rmsd) between C^{α} positions of the six subunits is in the range 0.07-0.12 Å.

Sequence building

The complete amino acid sequence of the *Cor. officinalis* VBPO is not currently known. The partial sequence information for the enzyme has shown that it is closely related to the two VBPOs from the red algae *Cor. pilulifera* (Shimonishi *et al.*, 1998) with over 90% identity for the five regions sequenced (C. Rush & J.A.L., unpublished data). The two amino acid sequences of the *Cor. pilulifera* enzymes were used as a basis for the side-chain assignments in the CVBPO X-ray structure.

No electron density was observed for the N-terminal Met1 in any subunit, although glycine residues at position 2 are clearly defined in the electron density in each subunit. This is in agreement with the N-terminal sequence of the CVBPO (C. Rush & J.A.L., unpublished data) where Met at position 1 was absent. The VBPO1 sequence from *Cor. pilulifera* has a two-residue insertion after position 49 and VBPO2 sequence has a one-residue insertion (Shimonishi *et al.*, 1998) after position 423. Neither of these insertions has been observed in the CVBPO electron density maps. The numbering of residues will be according to the CVBPO crystal model.

The electron density maps were calculated using phases from the CVBPO enzyme structure with zero side-chain occupancy of the residue in question in order to resolve the sequence ambiguities in the primary structure of the *Cor. officinalis* enzyme. The resulting $2F_o - F_c$ and $F_o - F_c$ maps were inspected in all six subunits. These maps were consistent with the consensus sequence between the two *Cor. pilulifera* enzymes for 534 amino acid residues out of 595 (89.7% of total). Ten amino acid residues in each subunit were assigned to a different residue type from the consensus sequence (Figure 1). Out of 51 sequence differences between the two enzymes of the *Cor. pilulifera*, 33 were resolved in favour of VBPO2, 13 in favour of VBPO1 and five were assigned a different amino acid type. An example of such an assignment is shown in Figure 2 for Asn419. This assignment was based not only on the shape of the electron density, but also on the H bonding which was not consistent with either Ile (VBPO1) or Lys (VBPO2).

The cloning and nucleotide sequencing of the CVBPO gene is in progress (J.A.L., unpublished data). Once this is complete, further refinement of the X-ray model will be carried out.

CVBPO structure

The CVBPO subunit (Figure 3) measures approximately 85 Å × 56 Å × 55 Å in size. It is folded into a single α + β type domain of 595 amino acid residues. The first ten N-terminal amino acid residues point away from the body of the domain which is composed of 19 α-helices from 6 to 26 residues in length. There are also eight 3_{10} helices and 14 β-strands. The β-strands are mainly involved in β-hairpins. One of the surfaces of the subunit is flat. The assignment of the CVBPO secondary structural elements is shown in Figure 1.

The CVBPO dimer is shown in Figure 4. The flat surfaces of the two subunits complement each other, covering an area of 5260 $Å^2$ or 20.5% of the subunit solvent accessible surface (AREAIMOL; CCP4, 1994). The residues 123-124 from one subunit and 368-369 from the other subunit in the dimer form a parallel two-stranded β-sheet. The β-hairpins 270-273 and 276-279 from each subunit in the dimer form an antiparallel four-stranded β-sheet. The vanadate-binding site is located at the bottom of the active-site cleft, which is about 20 Å deep and 14 Å wide. The active-site cleft is formed from residues of two different subunits in the dimer (Figure 4(b)). The residues of one subunit form the bottom of the cleft, and the top of the cleft is formed predominantly from the residues of the other subunit of the dimer. The involvement of residues from the neighbouring subunit in the active-site cleft would suggest that the CVBPO dimer is required to maintain specificity and stereoselectivity for halogenation of organic substrates, despite the fact that all vanadate-binding residues come from one subunit.

The CVBPO dodecamer measures ~150 Å in diameter. Some 12 subunits are arranged with 23 cubic point group symmetry (Figure 5). This symmetry has only been observed in two other enzyme structures to date, a DNA protection protein Dps from *Escherichia coli* (Grant *et al.*, 1998) and an ornithine carbamoyltransferase enzyme from *Pyrococcus furiosus* (Villeret *et al.*, 1998). Each of the cubic faces is made up of a dimer. The N-terminal region of each subunit contributes to the formation of the central cavity (Figure 6). The diameter of this cavity is about 26 Å and does not have any

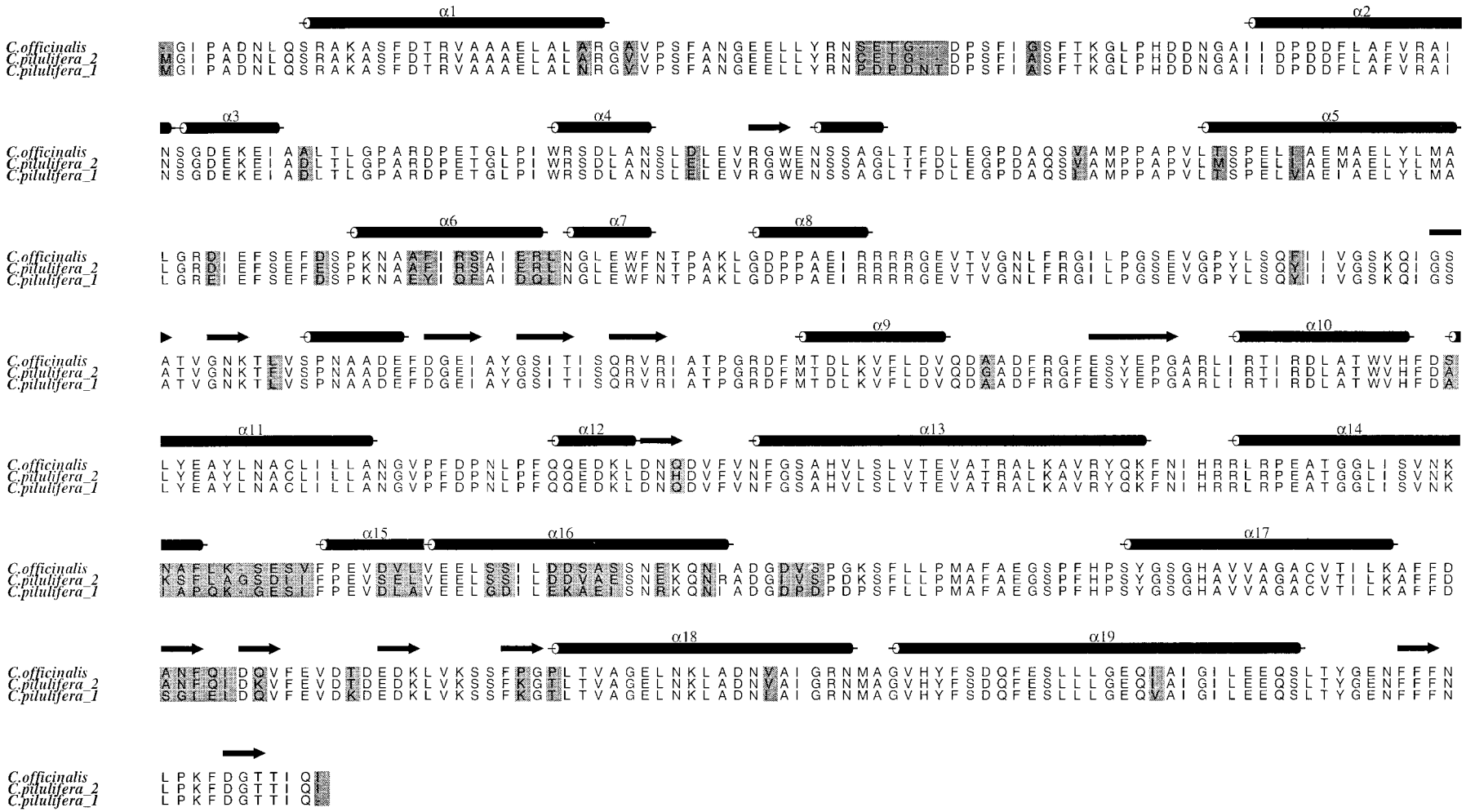

Figure 1. Alignment of the sequence as modelled into the X-ray structure of CVBPO to the two known sequences, VBPO1 and VBPO2, for *Cor. pilulifera*. Helices are shown as cylinders and β-strands are shown as arrows above the alignment. The α-helices are numbered from 1 to 19. The Figure was prepared using the program ALSCRIPT (Barton, 1993).

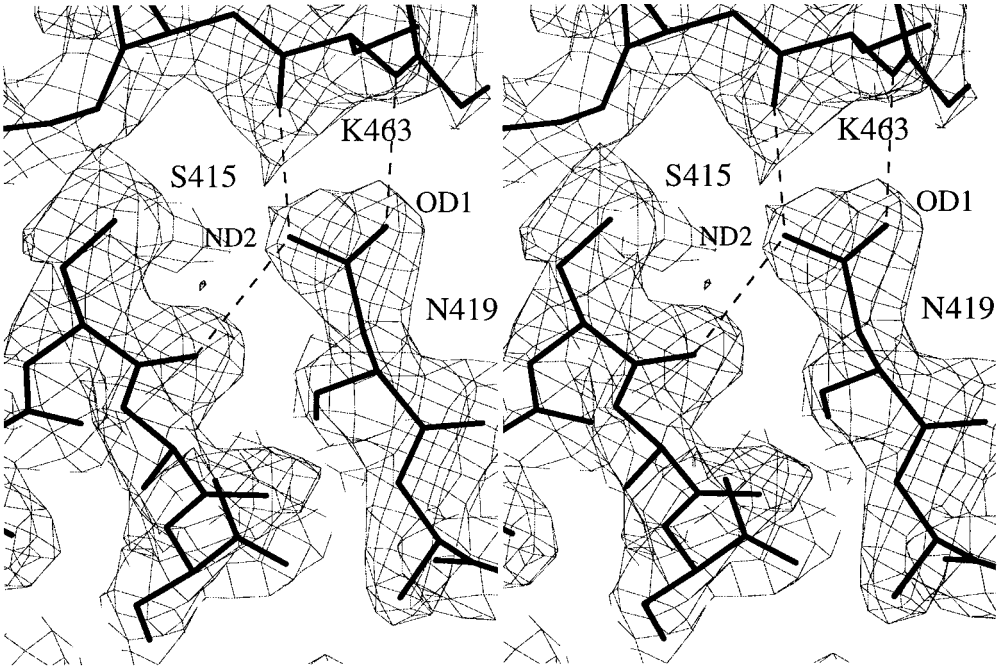

Figure 2. A stereo drawing of the $2F_o - F_c$ electron density map contoured at 1σ (0.36 e/Å^3) for the residue 419 in the CVBPO structure. The corresponding residue is Ile in the VBPO1 sequence and Lys in the VBPO2 sequence reported for *Cor. pilulifera* (Shimonishi *et al.*, 1998) as shown in Figure 1. The map was calculated using phases from the model in which the side-chain of this residue was omitted. The electron density and the H bonding pattern suggest this residue to be Asn. The Figures 2-6, 7(a), (b) and 8 were created using the program BOBSCRIPT (Kraulis, 1991; Esnouf, 1997).

specific charge or hydrophobic properties. This feature is therefore unlikely to bind metals and is proposed to have a structural role.

An additional 3245 Å^2 of the solvent accessible area of each subunit is buried upon dodecamer formation from dimers. This gives an overall figure of 8505 Å^2 for the buried area for each subunit, which amounts to 33.2% of its surface. Each subunit makes at least one H bond with nine other subunits within the dodecamer.

Active-site

The vanadium-binding site in the CVBPO is located on the bottom of a deep cavity formed by residues from both subunits. The bottom of the cleft is formed by the residues of helices α10, α11, α14, α17, α18, α19 of one subunit. The top of the cleft is formed by the residues of helix α9 and some loops from the same subunit and helices α11, α12 and α13, the β-hairpin (251-253 and 256-258) and the divalent cation binding motif (see below) of the neighbouring subunit. The long helix α11 contributes its residues to the active-site clefts of both subunits.

In this structure, the active site is occupied by inorganic phosphate which is known to compete with vanadate for binding to VBPO (Hemrika *et al.*, 1997). Unlike the vanadate group the phosphate group does not form a covalent bond with the active-site histidine residue (His551) because of the high energy of formation of such a bond (Figure 7(a)). The phosphate group is located at the N terminus of the helix α17 (Figure 7(b)) at the bottom of the cleft (see above) and is stabilised by its dipole moment, and H bonds with Ser483 OG, Gly484 N and His485 ND1. The His551, which is proposed to make a covalent bond to the vanadium atom is H bonded to one of the phosphate group oxygen atoms. Additionally, the phosphate group forms salt bridges with Lys398 (helix α13), Arg406 (helix α14) and Arg545 (helix α18).

The shape of the active-site cleft and charge distribution can be seen on the electrostatic surface diagram (Figure 7(c)). There are several hydrophobic patches and charged residues which could provide binding sites for the organic substrates. Attempts to co-crystallise CVBPO with various known organic substrates or halogen ions, or to obtain the complexes by soaking of the crystals are in progress.

Divalent cations

When solvent was being incorporated into the structure, all of the strong positive peaks in the $(F_o - F_c)$ maps were initially described as water molecules. After partial refinement, six water molecules had *B*-factors which were lower than the *B*-factors of the surrounding protein atoms. The peaks occupied the same position close to the dimer interface in all six subunits and had only

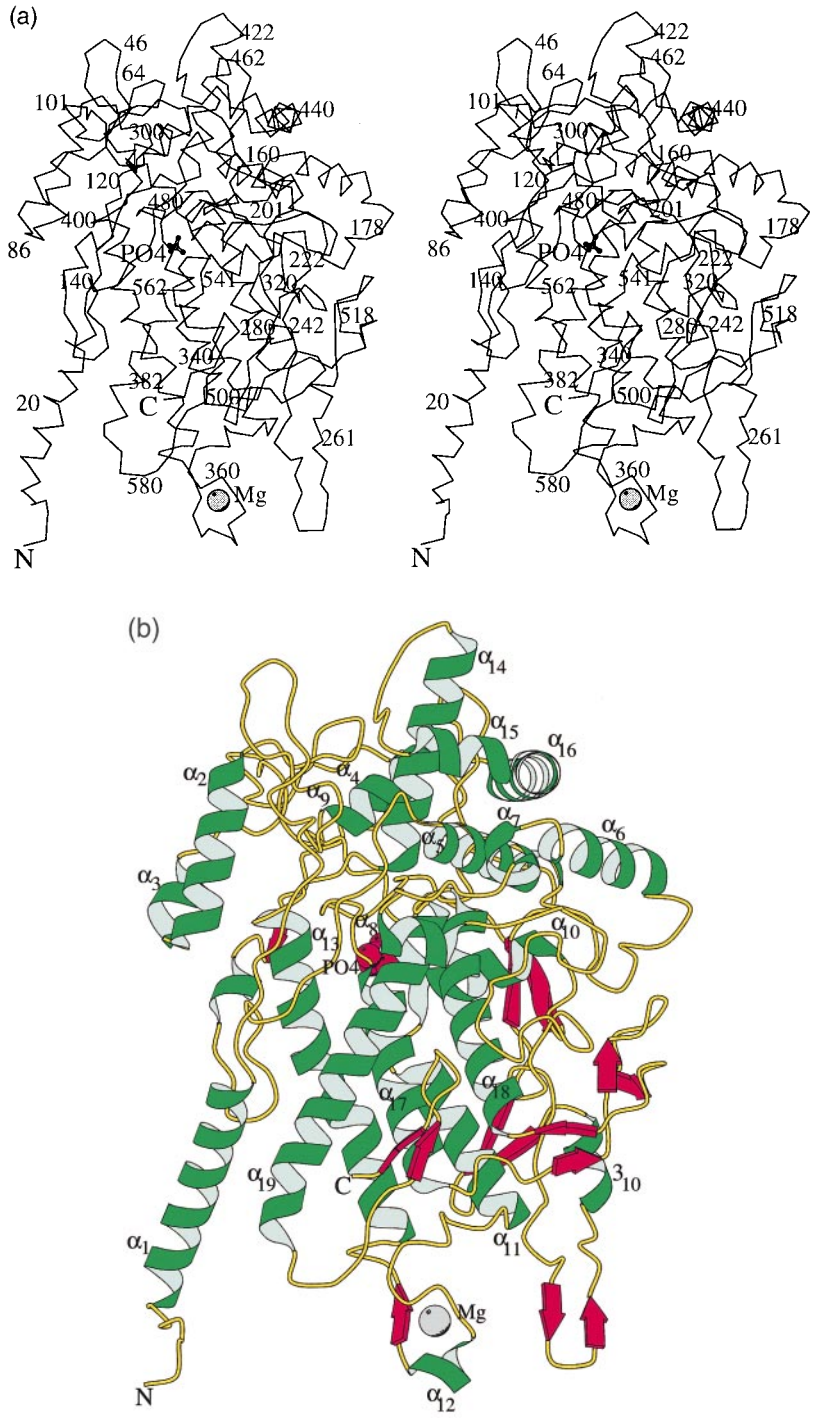

Figure 3. Structure of the CVBPO subunit. (a) A stereo view of the C^{α} trace. Each 20th residue is numbered. (b) Ribbon diagram of the subunit in the same orientation as in (a). α-Helices are numbered from 1 to 19. The inorganic phosphate ion bound at the vanadium site and the bound Mg^{2+} are shown as CPK space-filling models.

carbonyl and carboxyl enzyme groups in the first co-ordination sphere. As the mother liquor contained no added divalent metal ions, the sites are probably occupied by a mixture of magnesium and calcium ions, which were present in the mother liquor in trace amounts, or by *in vivo* divalent cations. When Mg^{2+} was introduced at these sites, the *B*-factors were comparable with those of the surrounding protein atoms. This suggests that a larger proportion of sites are occupied by Mg^{2+}. Previous results obtained using argon plasma emission spectroscopy of the *Cor. pilulifera* bromoperoxidase also suggested the presence of Mg^{2+} bound to the enzyme which could not be totally removed by exhaustive dialysis of the enzyme against a buffer containing 1 mM EDTA or *o*-phenanthroline (Itoh *et al.*, 1986).

The divalent cations bind close to the subunit interface in the dimer on the top of the active-site cleft (Figure 4(a)) in the α-helix 12/β-strand (368-369) motif. The Mg^{2+} is coordinated by main-chain oxygen atoms of Phe359, Gln361 and Gln368 and carboxyl groups of Asp363 and Asp366. The distance between the Mg^{2+} of one subunit of the

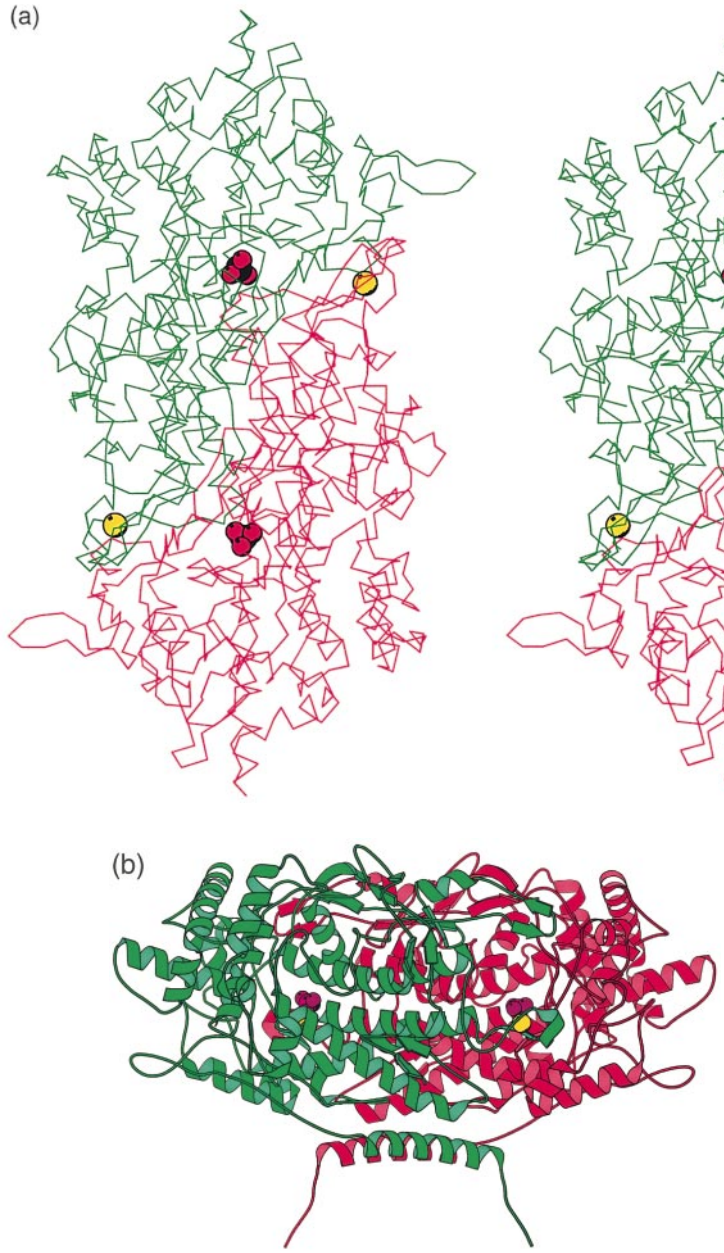

Figure 4. Structure of the CVBPO dimer. (a) A stereo diagram of the C^{α} trace viewed along the molecular dyad. The two subunits are shown in different colours. (b) A ribbon diagram representation viewed normal to the molecular dyad. The inorganic phosphate and Mg^{2+} are shown as CPK space-filling models.

dimer and the phosphorus atom of the inorganic phosphate bound at the active-site of the other subunit is 19 Å. Divalent cations seem to be necessary to maintain the structure of the active-site cleft and for dimer interaction. However, their direct involvement in the CVBPO reaction seems unlikely due to the large distance from the vanadate-binding site.

Comparison with other vanadium haloperoxidases

The structure of the chloroperoxidase from fungus *Cur. inaequalis* (Messerschmidt & Wever, 1996), which is a two-domain protein can be superimposed with the CVBPO dimer (Figure 8(a)). Many α-helices of each chloroperoxidase domain are structurally equivalent to some α-helices in the two different CVBPO subunits. This suggests a divergent evolutionary relationship between the CVBPO and the chloroperoxidase. It would appear that the CVBPO represents an ancestral enzyme with a two-subunit catalytic structure while the chloroperoxidase has undergone gene duplication, as suggested from its X-ray structure (Messerschmidt & Wever, 1996).

The CVBPO dimer and chloroperoxidase monomer can be superimposed with a rmsd value of 1.9 Å for 259 matching C^{α} atoms. The vanadate-binding domain of the chloroperoxidase superimposes with one of the CVBPO subunits with rmsd of 1.8 Å for 181 matching C^{α} atoms. The chloroperoxidase N-terminal domain superimposes with the other subunit of CVBPO with an rmsd value of

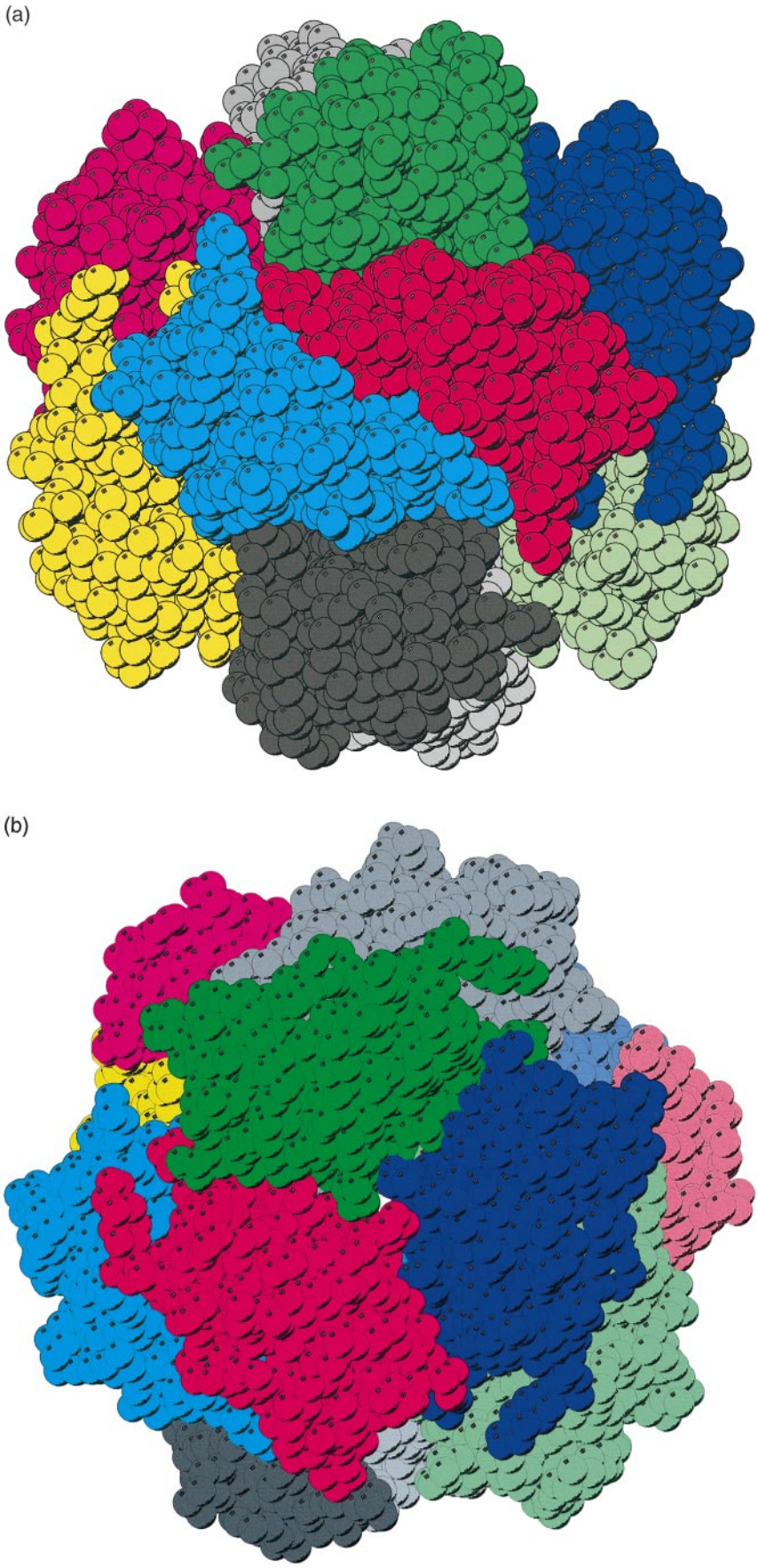

Figure 5. A space-filling model of the C^{α} trace of the CVBPO dodecamer viewed (a) along the molecular dyad and (b) along the molecular 3-fold axis. The individual subunits are shown in different colours.

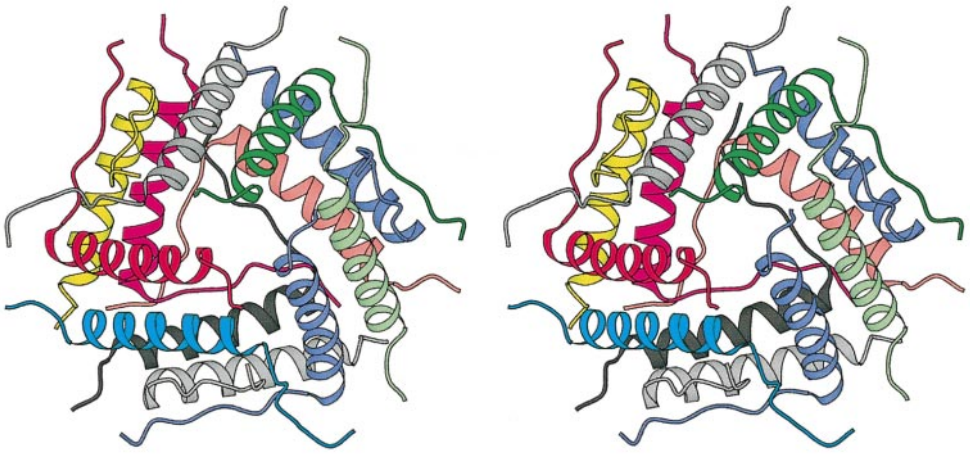

Figure 6. A stereo diagram showing the N-terminal residues (2-32) of each subunit of the CVBPO dodecamer which form a spherical cavity in the centre of the molecule. The view and colour code correspond to those shown in Figure 5(b).

1.6 Å for 78 matching atoms. The αB-helix of the chloroperoxidase N-terminal domain is structurally equivalent to α11 of one CVBPO subunit, αC to α13, αE to α17 and αG to α19. In the catalytic domain of chloroperoxidase, αi is equivalent to α5 of the other CVBPO subunit, αJ to α10, αK to α11, αL to α13, αM to α14, αN to α17, αO to α18 and αS to α19. Thus, not only four equivalent helices in both chloroperoxidase domains remain evolutionally conserved (those equivalent to α11, α13, α17 and α19 of CVBPO) but their relative position is also conserved. These helices form the vanadate-binding site of one CVBPO subunit and contribute to the active-site cavity of another subunit. The chloroperoxidase has lost the catalytic function of its N-terminal domain. It would appear that the chloroperoxidase C-terminal domain has retained structure and residues related to catalytic functions and has lost most of the features related to a second active site as it evoluted. Conversely, the N-terminal domain retained mainly features which contribute to the active-site cleft in the catalytic domain and lost features of its own active site. However, the number of residues per catalytic site has remained similar (595 in CVBPO and 609 in the chloroperoxidase).

Since the coordinates for the VBPO from *A. nodosum* (Weyland *et al.*, 1999) are not publicly available, the comparison of AVBPO and CVBPO enzymes which have 33% amino acid sequence identity will only be limited to the data which have been published. The amino acid sequence of the AVBPO is 39 residues shorter than that of the CVBPO. The sequence alignment of the two enzymes suggests that the *A. nodosum* enzyme extends seven amino acid residues at the N terminus and 25 amino acid residues at the C terminus. This results in several deletions of up to 20 residues in length in the AVBPO in comparison with the CVBPO. Thus, although most of the long α-helices which make up the core of the molecule seem to be conserved between the two enzymes, many small helices and β-strands which are on the surface differ between the two structures (Figure 1; Table 1 of Weyand *et al.*, 1999). To avoid confusion, α-helices are listed in numerical order for the *Cor. officinalis* structure and not in alphabetical order as in AVBPO. The αF, αG and αP-helices of *A. nodosum* VBPO are not observed in the *Cor. officinalis* structure, and α4, α8, α12 and several 3_{10} helices are not observed in *A. nodosum*. The number and location of the β-strands is also different between the two structures. The divalent cations do not occur in the AVBPO structure and indeed the α-helix/β-strand cation binding feature of CVBPO is also not observed in the *A. nodosum*

Table 1. Summary of data collection and model refinement statistics

Final R_{cryst} [a] (22-2.3 Å) (%)	17.2
R_{free} (2.0% total data) (%)	22.7
No. of protein residues	3570
Average *B*-factor protein (Å^2)	18.4
No. of water molecules	2192
Average *B*-factor waters (Å^2)	25.7
r.m.s. deviations from ideality (target values are given in parentheses)	
Bond lengths (Å)	0.012 (0.020)
Bond angles (Å)	0.031 (0.040)
1-4 neighbours (Å)	0.035 (0.050)
Planar groups (Å)	0.021 (0.025)
Torsion angles (deg.)	
Planar	3.4 (7.0)
Staggered	14.0 (15.0)
Orthonormal	29.1 (20.0)
B-factors correlation (Å^2)	
Main-chain bond	2.1 (4.0)
Main-chain angle	2.9 (6.0)
Side-chain bond	5.6 (8.0)
Side-chain angle	6.8 (10.0)

[a] $R_{cryst} = \Sigma||F_o| - |F_c||/\Sigma|F_o|$.

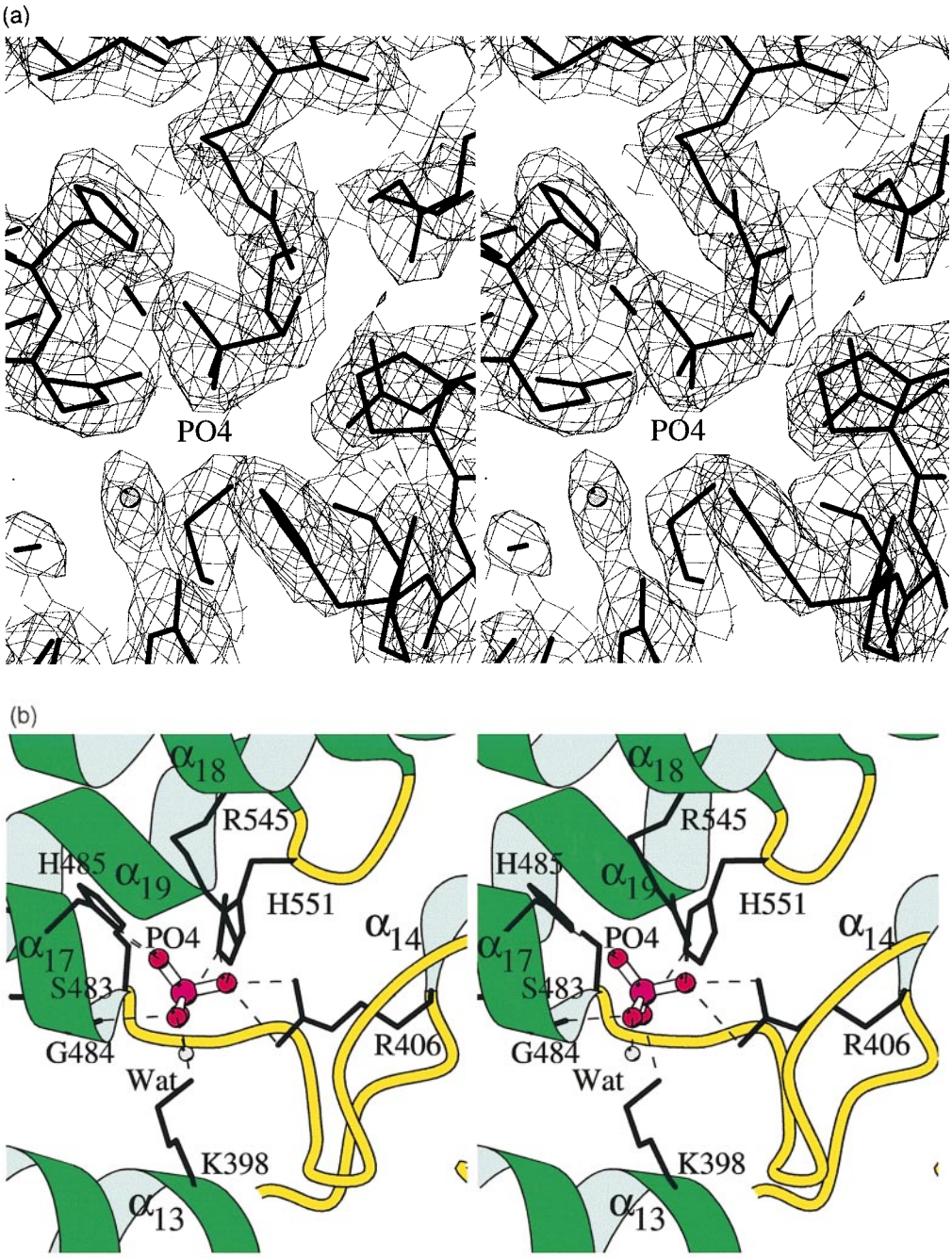

Figure 7. (*legend opposite*)

enzyme which has a three-residue deletion in this region.

Both AVBPO and CVBPO show a high level of thermostability as well as stability to organic solvents and to high concentrations of hydrogen peroxide (Weyand *et al.*, 1999; Sheffield *et al.*, 1993). The thermostability of these enzymes, which come from mesophilic organisms, is unexpected and could be due to an adaptation to harsh environmental conditions of overheating and dehydration which the algae endure at low tide. It also could result from the necessity of the enzyme to be stable to the chemically active substrate hydrogen peroxide and to the hypohalide groups which are intermediates/products of the VBPO reaction. It seems that the two enzymes have developed different mechanisms of stability. In the dimeric AVBPO enzyme all of the cysteine residues are involved in three intersubunit and one intrasubunit disulphide bonds, which make a significant contribution to the enzyme stability. None of these cysteine residues is conserved in CVBPO. The only two cysteine residues in CVBPO are located far apart from one another and are observed in the reduced

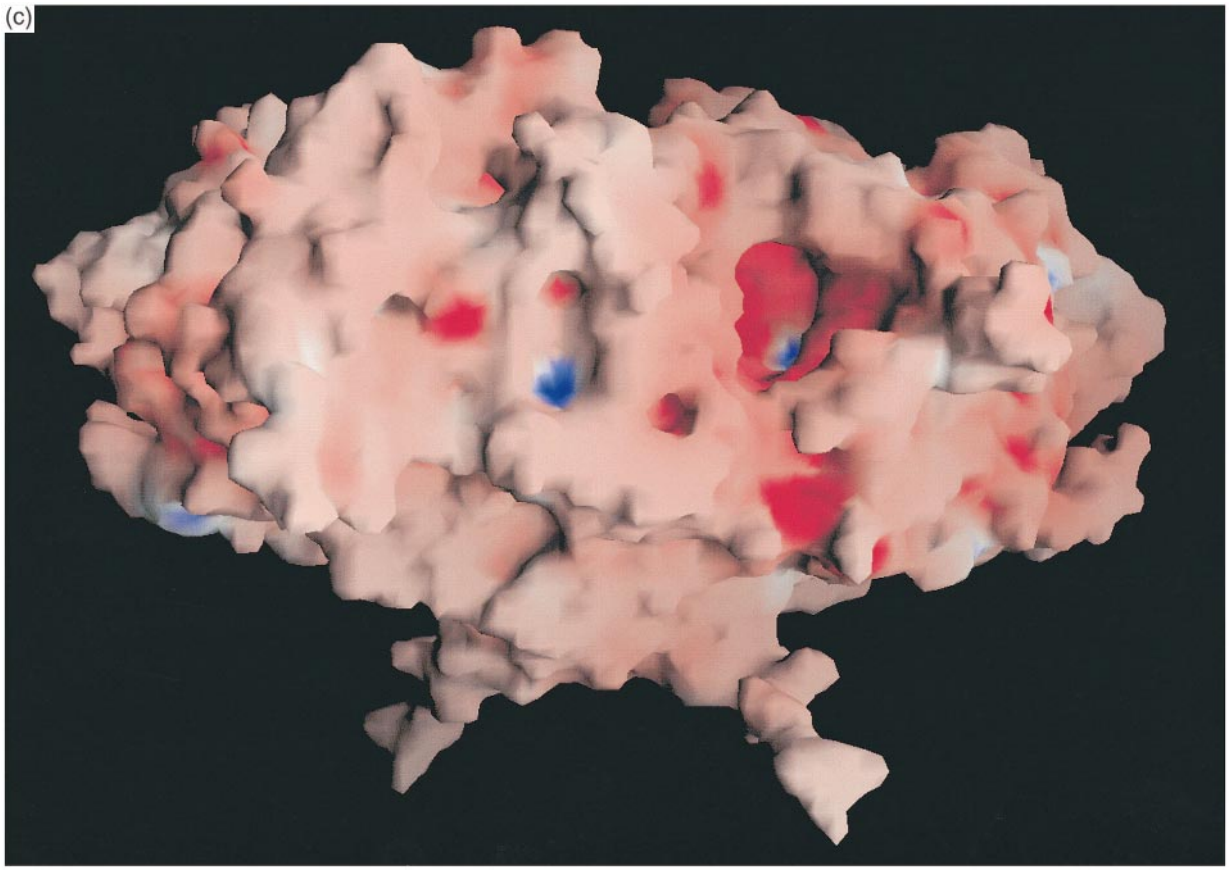

Figure 7. The active site of the CVBPO enzyme. (a) The $2F_o - F_c$ electron density contoured at 1σ is shown around the vanadate binding site occupied by the inorganic phosphate group (PO4). (b) A stereo ribbon diagram of the active site viewed from the outside. The phosphate ion is shown as a ball and stick model. Amino acid residues surrounding this site are shown as filled bonds. (c) The electrostatic potential surface of the CVBPO dimer viewed as in Figure 4(b). Positive charge is shown in blue and negative charge in red. The large active-site cleft can be seen on the right-hand side of the Figure. The drawing was prepared using the program GRASP (Nicholls *et al.*, 1991).

form. The stability of CVBPO seems to result from the high dodecameric oligomerisation which buries an extra 12% of the subunit solvent accessible area and from the binding of the divalent cations.

The presented structure of CVBPO agrees with the mechanisms of halogenation proposed (Messerschmidt & Wever, 1996; Hemrika *et al.*, 1999; Weyand *et al.*, 1999). All of the residues involved in the vanadate binding are conserved between the two algal bromoperoxidase molecules and the vanadium chloroperoxidase molecule from the fungus *Cur. inaequalis* (Figure 8(b)). Only five residues out of 17 lining the wall of the active-site cavity and not involved in the vanadate binding are conserved between CVBPO and AVBPO, Asp333 (Asp278), Glu473 (Glu406), Pro476 (Pro409), His478 (His411), from the vanadate binding subunit, and Phe371 (Phe315) from the neighbouring subunit. None of these five residues is structurally conserved in the *Cur. inaequalis* chloroperoxidase structure. His478 is located at the position of Phe397 which was suggested to bind the chloride ion in the chloroperoxidase active site (Messerschmidt & Wever, 1996). This substitution and H bonding of Asp333 (Asp278) to the catalytic His485 (His418) were suggested to be the reasons for a preference for bromination rather than chlorination for AVBPO (Weyand *et al.*, 1999) and indeed His478 and Asp333 are conserved in all VBPOs. An active-site serine residue was suggested as a possible candidate to form a carbon-bromine covalent bond from EXAFS studies (Dau *et al.*, 1999). However, the solvent accessibility of this Ser483 in CVBPO (Ser416 in AVBPO) seems to be low in the phosphate-bound form of the enzyme. The significant structural changes within the active site during the catalytic cycle which would make it accessible have been ruled out for the chloroperoxidase enzyme on the basis of structural studies on mutants proteins (Macedo-Ribeiro *et al.*, 1999).

Only three hydrophilic residues and no charged residues except those involved in the vanadate binding are observed within 7.5 Å from the vanadate O^4 oxygen atom in the *A. nodosum* structure (Weyand *et al.*, 1999). There are three charged residues, Glu124, Arg395 and Asp292, within approximately the same sphere in CVBPO. These residues

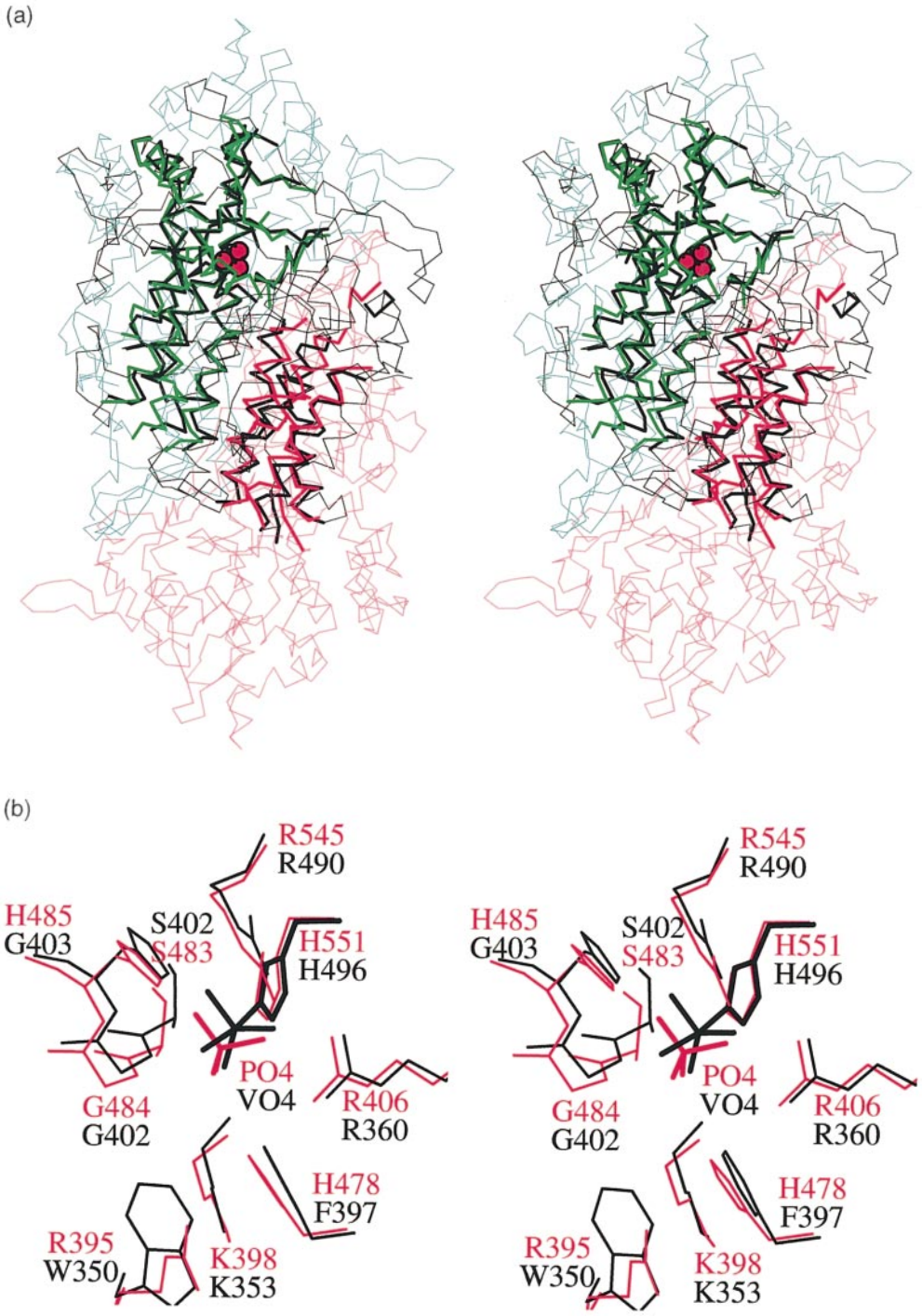

Figure 8. A structural comparison of CVBPO and the holo vanadium chloroperoxidase from *Cur. inaequalis* (Messerschmidt & Wever, 1996; PDB code 1VNI). (a) A superposition of the C^{α} trace of the CVBPO dimer (subunits are shown in red and green) with the chloroperoxidase monomer (black). The residues which structurally superimpose in both structures are shown in thicker lines. The superposition was made and refined using the program O (Jones *et al.*, 1991). Also shown is a CPK space-filling model of the vanadate found in chloroperoxidase. The view is the same as in Figure 4(a). (b) The superposition of the active sites of the CVBPO enzyme (shown in red) and the chloroperoxidase (shown in black). The structures are superimposed as in (a). In the centre of the picture are shown vanadate which makes a covalent bond to NE2 of His496 in the chloroperoxidase and inorganic phosphate bound at the vanadate site in CVBPO. Side-chains for residues implicated in the catalytic mechanism are shown as bonds and labelled in the respective colour. The conserved residues or those with similar locations are shown.

could affect the substrate specificity and stereoselectivity of the reaction.

The results reported here form the basis for future investigations on the structure-function relationships of CVBPO, including the solution and analysis of the structure with vanadate in the active site and with substrates and reaction intermediates.

Materials and Methods

Crystallisation and data collection

The CVBPO enzyme was purified and crystallised as described (Brindley *et al.*, 1998). The crystals grew from 0.1 M Tris-HCl and 2 M ammonium dihydrogen phosphate at pH 5.0 using the hanging drop vapour phase diffusion technique. Their space group was determined as tetragonal $P4_222$ with unit cell dimensions $a = b = 201.9$ Å, $c = 178.1$ Å. The crystals were harvested into a mother liquor containing 2.2 M ammonium dihydrogen phosphate at pH 5.0. Native data were collected from a single crystal at room temperature on the EMBL X31 beamline at the Hamburg synchrotron to 2.3 Å resolution at 0.93 Å wavelength. Cryocooling was not used due to a large increase in the mosaicity of the crystals upon freezing. The crystal used for a native data collection was later soaked for one hour in mother liquor containing 10 mM mercury acetate. This derivative data were collected to 2.5 Å resolution on the same beamline at 0.99 Å wavelength, in order to optimise the anomalous signal of the mercury. The data were processed using DENZO and SCALEPACK (Otwinowski & Minor, 1997).

The Patterson function

The native Patterson map contained a peak 44% the height of the origin at $u = v = 1/2$, $w = 0$ when calculated at 10-4 Å resolution . If this pseudotranslation is assumed to be a proper crystallographic translation, then the crystal data can be re-indexed into a smaller tetragonal $P4_222$ unit cell with $a = b = 142.8$ Å. These cell parameters are $\sqrt{2}$ times smaller than those of a full cell (201.9 Å). The re-indexing of the data into a smaller cell is effectively the averaging of the two molecules related by the pseudotranslation. Due to computer hardware limitations most of the calculations were carried out in this so-called reduced cell.

Phasing

The asymmetric unit of the reduced cell contains three CVBPO subunits. The three mercury sites per subunit (nine in the asymmetric unit of the reduced cell) were found using an isomorphous difference Patterson search implemented in SHELX (Sheldrick, 1991) at the 10-6 Å resolution range. The heavy atom positions confirmed the 23-point group symmetry of the CVBPO molecule suggested from the self-rotation function (Brindley *et al.*, 1998). Non-crystallographic symmetry operators were determined from the heavy atom positions. The heavy atom positions, occupancies, anomalous occupancies and *B*-factors were refined by MLPHARE (Otwinowski, 1991; CCP4, 1994). The resulting figure of merit of the heavy atom phases was 0.31 to 3 Å (Table 2). The phases were improved by threefold NCS averaging of the SIR electron density at 2.5 Å using DM (Cowtan, 1994).

Table 2. Summary of data collection and phasing statistics

Data set	Native	Mercury acetate
Resolution range (Å)	20-2.3 (2.34-2.3)[a]	20.0-2.5 (2.54-2.5)[a]
Completeness (%)	96.8 (95.2)[a]	99.7 (99.7)[a]
R_{sym}	0.157 (0.513)[a]	0.164 (0.538)[a]
$\langle I\rangle/\langle\sigma I\rangle$	6.62 (2.3)[a]	9.3 (2.77)[a]
Redundancy	3.1 (2.3)[a]	5.0 (4.7)[a]
Unique reflections	156,862	126,445
B-factor of data from Wilson plot (Å^2)	21.5	27.7
MFID		0.168
Number of sites		9[b]
Phasing power		1.28[b]
R_{cullis}		0.72[b]
FOM		0.31[b]

[a] Values in parentheses are given for the outer resolution shell.

[b] Phasing statistics are given for 10-3 Å resolution and for the so-called ''reduced'' cell (see Materials and Methods).

$R_{sym} = \Sigma_h\Sigma_J|\langle I_h\rangle - I_J(h)|/\Sigma_h\Sigma_J I(h)$, where $I(h)$ is the intensity of reflection h. Σ_h is the sum over all reflections and Σ_J is the sum over J measurements of the reflection. MFID is the mean fractional isomorphous difference, $\Sigma||F_P| - |F_{PH}||/\Sigma|F_P|$, where F_P are the native structures factors and F_{PH} the derivative structure factors. Phasing power $= F_H/E$, where E is estimated lack of closure error. R_{cullis} = lack of closure error/isomorphous difference and is quoted for centric reflections only. FOM is the overall Figure of merit, defined as the estimated cosine of phase error.

Model building

One subunit was built at this stage using the program O (Jones *et al.*, 1991). The asymmetric unit contents of the reduced cell were obtained by applying NCS transformations to this subunit. The partial structure was refined using external phases as implemented in REFMAC (Murshudov *et al.*, 1997) in order to increase the convergence radius of the refinement. Partial model and heavy atom phases were combined by REFMAC and averaged by DM. About 520 residues out of 595 were built in the reduced cell before transferring the model to the full unit cell for final refinement. Main-chain atoms of all 595 residues are clearly defined in the electron density in the full cell. Water molecules were added using ARP (Lamzin & Wilson, 1993). The vanadate site in each subunit is occupied by a phosphate ion. One magnesium ion per subunit has been identified on the basis of its *B*-factor and co-ordination. Some of the amino acid sequence ambiguities were resolved at the final stages of refinement.

Pseudosymmetry

The centre of mass of the refined CVBPO dodecamer is located at (1/4, 1/4, 1/4) in the full cell. One of the dodecamer molecular dyads coincides with a diagonal crystallographic 2-fold axis. The other molecular dyad makes an angle 1.25° with the 4-fold crystallographic axis. This small deviation from the crystallographic symmetry causes the strong Patterson function peak at $u = v = 1/2$, $w = 0$ (see above). The re-indexing of data into the reduced cell introduced a co-ordinate error of up to 1.65 Å for the atoms which are most remote from the crystallographic dyad. The heavy atom location at 6 Å

was not influenced by this co-ordinate error. However, phasing at 3 Å and the density modification at 2.5 Å were affected. Fortunately, the co-ordinate error introduced by re-indexing of the data was smaller for a subunit which belongs to a dimer related by a crystallographic dyad, since it lies closer to this dyad. This allowed the building of most of this subunit in the reduced cell. To summarise, the most computationally demanding steps of the structure determination can be accelerated in the reduced cell for which pseudosymmetry is treated as a proper crystallographic symmetry. The resulting phases are correct within the certain resolution limit which is determined by the deviation of the pseudosymmetry from the assumed crystal symmetry. This approach in the case of CVBPO gave reasonably good phases up to 3 Å resolution. These phases were then extended to the whole data set by the refinement in the proper unit cell.

Data deposition

The structure factors and refined coordinates of the *Cor. officinalis* bromoperoxidase have been deposited with the RCSB Brookhaven Protein Data Bank (Bernstein *et al*., 1977); the access code is 1QHB.

Acknowledgements

We thank Andrey Lebedev for comments on the manuscript. This work was supported by grants from the BBSRC as postdoctoral fellowships to M.N.I. and A.R.D. We also thank the European Union for support of the work at EMBL Hamburg through the HCMP Access to Large Installations Project, contract no. CHGE-CT93-0040.

References

Ahern, T. J., Allan, G. G. & Medcalf, D. G. (1980). New bromoperoxidases of marine origin: partial purification and characterization. *Biochim. Biophys. Acta,* **616**, 329-339.

Anderson, M., Willetts, A. & Allenmark, S. (1997). Asymmetric sulfoxidation catalyzed by a vanadium-containing bromoperoxidase. *J. Org. Chem.* **62**, 8455-8458.

Barnett, P., Hemrika, W., Dekker, H. L., Muijsers, A. O., Renirie, R. & Wever, R. (1998). Isolation, characterization and primary structure of the vanadium chloroperoxidase from the fungus *Embellisia didymospora*. *J. Biol. Chem.* **273**, 23381-23387.

Barton, G. J. (1993). Alscript - a tool to format multiple sequence alignments. *Protein Eng.* **6**, 37-40.

Bernstein, F. C., Koetzle, T. F., Williams, G. J. B., Meyer, E. J., Brice, M. D., Rogers, J. K., Kennard, O., Shimanouchi, T. & Tasumi, M. (1977). The Protein Data Bank: a computer based archival file for macromolecular structures. *J. Mol. Biol.* **112**, 535-542.

Brindley, A. A., Dalby, A. R., Isupov, M. N. & Littlechild, J. A. (1998). Preliminary X-ray analysis of a new crystal form of the vanadium-dependent bromoperoxidase from *Corallina officinalis*. *Acta Crystallog. sect. D,* **54**, 454-457.

Collaborative Computational Project No 4 (1994). The CCP4 suite: programs for protein crystallography. *Acta Crystallog. sect. D,* **50**, 760-763.

Coughlin, P., Roberts, S., Rush, C. & Willetts, A. (1993). Biotransfomation of alkenes by haloperoxidases: regiospecific bromohydrin formation from cinnamyl substrates. *Biotech. Letters,* **15**, 907-912.

Cowtan, K. D. (1994). DM: an automated procedure for phase improvement by density modification. In *CCP4 Newsletter on Protein Crystallography. no 31* (Bailey, S. & Wilson, K., eds), pp. 34-38, Daresbury Laboratory, Warrington, UK.

Dau, H., Dittmer, J., Epple, M., Hanss, J., Kiss, E., Rehder, D., Schulzke, C. & Vilter, H. (1999). Bromine K-edge EXAFS studies of bromide binding to bromoperoxidase from *Ascophyllum nodosum*. *FEBS Letters,* **457**, 237-240.

Esnouf, R. M. (1997). An extensively modified version of Molscript that includes greatly enhanced colouring capabilities. *J. Mol. Graph. Model.* **15**, 132.

Grant, R. A., Filman, D. J., Finkel, S. E., Kolter, R. & Holge, J. M. (1998). The crystal structure of Dps, a ferritin homolog that binds and protects DNA. *Nature Struct. Biol.* **5**, 294-303.

Gribble, G. W. (1992). Naturally occurring organohalogen compounds - a survey. *J. Nat. Products,* **55**, 1353-1395.

Hemrika, W., Renirie, R., Dekker, H. L., Barnett, P. & Wever, R. (1997). From phosphatases to vanadium peroxidases: a similar architecture of the active site. *Proc. Natl Acad. Sci. USA,* **94**, 2145-2149.

Hemrika, W., Renirie, R., Macedo-Ribeiro, S., Messerschmidt, A. & Wever, R. (1999). Heterologous expression of the vanadium-containing chloroperoxidase in *Saccharomyces cerevisiae* and site-directed mutagenesis of the active site residues His496, Lys353, Arg360 and Arg490. *J. Biol. Chem.* **274**, 23820-23827.

Itoh, N., Izumi, Y. & Yamada, H. (1986). Characterisation of nonheme type bromoperoxidase in *Corallina pilulifera*. *J. Biol. Chem.* **261**, 5194-5200.

Itoh, N., Izumi, I. & Yamada, H. (1987). Haloperoxidase-catalysed halogenation of nitrogen-containing heterocycles represented by nucleic bases. *Biochemistry,* **26**, 282-289.

Itoh, N., Hasan, A. K. M. Q., Izumi, Y. & Yamada, H. (1988). Substrate specificity, regiospecificity and stereospecificity of halogenation reactions catalysed by non-heme-type bromoperoxidase of *Corallina pilulifera*. *Eur. J. Biochem.* **172**, 477-484.

Itoh, N., Morinaga, N. & Kouzai, T. (1994). Purification and characterization of a novel metal-containing nonheme bromoperoxidase from *Pseudomonas putida*. *Biochim. Biophys. Acta,* **1207**, 208-216.

Jones, T. A., Zou, J.-Y., Cowan, S. W. & Kjeldgaard, M. (1991). Improved methods for building protein models in electron density maps and the location of errors in these models. *Acta Crystallog. sect. D,* **50**, 157-163.

Kraulis, P. J. (1991). MOLSCRIPT: a program to produce both detailed and schematic plots of protein structures. *J. Appl. Crystallog.* **24**, 946-950.

Kusthardt, U., Hedman, B., Hodgson, K. O., Hahn, R. & Vilter, H. (1993). High-resolution XANES studies on vanadium-containing haloperoxidase: pH-dependence and substrate binding. *FEBS Letters,* **329**, 5-8.

Lamzin, V. S. & Wilson, K. S. (1993). Automated refinement of protein models. *Acta Crystallog. sect. D,* **49**, 129-147.

Laskowski, R. A., MacArthur, M. W., Moss, D. S. & Thornton, J. M. (1993). PROCHECK: a program to

check the stereochemical quality of protein structures. *J. Appl. Crystallog.* **26**, 283-291.

Macedo-Ribeiro, S., Hemrika, W., Renirie, R., Wever, R. & Messerschmidt, A. (1999). X-ray crystal structures of active site mutants of the vanadium-containing chloroperoxidase from the fungus *Curvularia inequalis*. *J. Biol. Inorg. Chem.* **4**, 209-219.

Manthey, J. A. & Hager, L. P. (1981). Purification and properties of bromoperoxidase from *Penicillus capitatus*. *J. Biol. Chem.* **256**, 11232-11238.

Messerschmidt, A. & Wever, R. (1996). X-ray structure of a vanadium-containing enzyme: chloroperoxidase from the fungus *Curvularia inaequalis*. *Proc. Natl Acad. Sci. USA,* **93**, 392.

Messerschmidt, A., Prade, L. & Wever, R. (1997). Implications for the catalytic mechanism of the vanadium-containing enzyme chloroperoxidase from the fungus *Curvularia inaequalis* by X-ray structures of the native and peroxide form. *Biol. Chem.* **378**, 309-315.

Murshudov, G. N. & Dodson, E. J. (1997). Simplified error estimation *a la* Cruickshank in macromolecular crystallography. In *CCP4 Newsletter on Protein Crystallography. no 33* (Winn, M., ed.), pp. 31-39, Daresbury Laboratory, Warrington, UK.

Murshudov, G. N., Vagin, A. A. & Dodson, E. J. (1997). Refinement of macromolecular structures by maximum-likelihood method. *Acta Crystallog. sect. D,* **53**, 240-255.

Neidleman, S. L. & Geigert, J. (1987). Biological halogenation: roles in nature, potential in industry. *Endeavour,* **11**, 5-15.

Nicholls, A., Sharp, K. & Honig, B. H. (1991). Protein folding and association: insights from the interfacial and hydrodynamic properties of hydrocarbons. *Proteins: Struct. Funct. Genet.* **11**, 281-296.

Otwinowski, Z. (1991). Maximum likelihood refinement of heavy atom parameters. In *Isomorphous Replacement and Anomalous Scattering* (Wolf, W., Evans, P. R. & Leslie, A. G. W., eds), pp. 80-86, Daresbury Laboratory, Warrington, UK.

Otwinowski, Z. & Minor, W. (1997). Processing of X-ray diffraction data collected in oscillation mode. *Methods Enzymol.* **276**, 307-326.

Plat, H., Krenn, B. E. & Wever, R. (1987). The bromoperoxidase from the lichen *Xanthoria parientina* is a novel vanadium enzyme. *Biochem. J.* **248**, 277-279.

Ramakrishan, C. & Ramachandran, G. N. (1965). Stereochemical criteria for polypeptide and protein chain conformation. *Biophys. J.* **5**, 909-933.

Rush, C., Willetts, A., Davies, G., Dauter, Z., Watson, H. & Littlechild, J. (1995). Purification, crystallisation and preliminary X-ray analysis of the vanadium-dependent haloperoxidase from *Corallina officinalis*. *FEBS Letters,* **359**, 244-246.

Sheffield, D. J., Harry, T. R., Smith, A. J. & Rogers, L. J. (1993). Purification and characterisation of the vanadium dependent bromoperoxidase from the macroalga *Corallina officinalis*. *Phytochemistry,* **32**, 21-26.

Sheffield, D. J., Harry, T. R., Smith, A. J. & Rogers, L. J. (1995). *Corallina officinalis* bromoperoxidase immobilized on agarose. *Phytochemistry,* **38**, 1103-1107.

Sheldrick, G. M. (1991). Heavy atom location using SHELXS-90. In *Isomorphous Replacement and Anomalous Scattering* (Wolf, W., Evans, P. R. & Leslie, A. G. W., eds), pp. 23-38, Daresbury Laboratory, Warrington, UK.

Shimonishi, M., Kuwamoto, S., Inoue, H., Wever, R., Ohshiro, T., Izumi, Y. & Tanabe, T. (1998). Cloning and expression of the gene for a vanadium-dependent bromoperoxidase from a marine macro-alga, *Corallina pilulifera*. *FEBS Letters,* **428**, 105-110.

Simons, E. C., Barnett, P., Vollenbroek, E. G., Dekker, H. L., Muijsers, A. O., Messerschmidt, A. & Wever, R. (1995). Primary structure and characterization of the vanadium chloroperoxidase from the fungus *Curvularia inaequalis*. *Eur. J. Biochem.* **229**, 566-574.

Soedjak, H. S. & Butler, A. (1990). Chlorination catalyzed by vanadium bromoperoxidase. *Inorg. Chem.* **29**, 5015-5017.

Van Peé, K. H. & Lingens, F. (1985). Purification and molecular and catalytic properties of bromoperoxidase from *Streptomyces phaeochromogenes*. *J. Bacteriol.* **161**, 1171-1175.

Van Schijndel, J. W., Vollenbroek, E. G. & Wever, R. (1993). The chloroperoxidase from the fungus *Curvularia inaequalis* - a novel vanadium enzyme. *Biochim. Biophys. Acta,* **1161**, 249-256.

Villeret, V., Clantin, B., Tricot, C., Legrain, C., Roovers, M., Stalon, V., Glansdorff, N. & Van Beeumen, J. (1998). The crystal structure of *Pyrococcus furiosus* ornithine carbamoyltransferase reveals a key role for oligomerization in enzyme stability at extremely high temperatures. *Proc. Natl Acad. Sci. USA,* **95**, 2801-2806.

Vilter, H. (1995). Vanadium-dependent haloperoxidases. *Met. Ions Biol. Syst.* **31**, 325-362.

Vreeland, V., Ng, K. L. & Epstein, L. (1998). cDNA sequence and active recombinant vanadium bromoperoxidase from *Fucus* embryos. *Mol. Biol. Cell*, **9**, 1043.

Wever, R., Plat, H. & de Boer, E. (1985). Isolation procedure and some properties of the bromoperoxidase from *Ascophyllum nodosum*. *Biochim. Biophys. Acta,* **830**, 181-186.

Wever, R., Krenn, B. E., De Boer, E., Offenberg, H. & Plat, H. (1988). Structure and function of vanadium-containing bromoperoxidases. *Prog. Clin. Biol. Res.* **274**, 477-493.

Weyand, M., Hecht, H., Kiess, M., Liaud, M., Vilter, H. & Schomburg, D. (1999). X-ray structure determination of a vanadium-dependent haloperoxidase from *Ascophyllum nodosum* at 2.0 Å resolution. *J. Mol. Biol.* **293**, 595-611.

Zeng, J. & Fenna, R. E. (1992). X-ray structure of canine myeloperoxidase at 3 Å resolution. *J. Mol. Biol.* **226**, 185-207.

Edited by R. Huber

(Received 8 February 2000; received in revised form 19 April 2000; accepted 25 April 2000)